C. R. Mecanique 342 (2014) 389–402

Contents lists available at ScienceDirect

Comptes Rendus Mecanique

www.sciencedirect.com

Separation flow control

Experimental detection of flow separation over a plain flap by wall shear stress analysis with and without steady blowing

Détection expérimentale du décollement de l'écoulement sur un volet sans fente par l'analyse du frottement pariétal avec ou sans soufflage continu

Timothée Chabert *, Julien Dandois, Éric Garnier, Laurent Jacquin

Onera – The French Aerospace Lab, 8, rue des Vertugadins, 92190 Meudon, France

ARTICLE INFO

Article history:
Received 2 September 2013
Accepted 27 January 2014
Available online 18 June 2014

Keywords:
Flow separation
Flow control
Flap
Steady blowing

Mots-clés :
Décollement
Contrôle des écoulements
Volet
Soufflage continu

ABSTRACT

The present article deals with the flow separation detection over a plain flap at a Reynolds number of $2 \cdot 10^6$ by the analysis of the wall shear stress fluctuations. Natural flow separation is first considered with the study of the evolution of wall shear stress fluctuations measured along the flap chord when the flap deflection angle is progressively increased. Then, steady blowing is applied and its effect on wall shear stress fluctuations is analysed. For both controlled and uncontrolled cases, flow separation criteria are defined, studied and compared.

RÉSUMÉ

Cet article traite de la détection du décollement de l'écoulement sur un volet sans fente pour un nombre de Reynolds de $2 \cdot 10^6$ par l'analyse des fluctuations du frottement pariétal. On considère en premier lieu le décollement naturel à travers l'étude de l'évolution des fluctuations de frottement pariétal mesurées sur la corde du volet lorsque son angle de braquage augmente progressivement. Par la suite, un contrôle par soufflage continu est appliqué et l'effet de ce contrôle sur les fluctuations de frottement pariétal est étudié. Dans les cas contrôlé et non contrôlé, des critères de décollement sont définis, étudiés et comparés entre eux.

1. Introduction

Measurement of wall shear stress has been hardly used to detect flow separation occurring on aerofoils since the early studies of Stack et al. [1] and Nakayama et al. [2]. Shear stress can be measured by non-intrusive devices such as hot films, however. This is particularly interesting for studies aiming at detecting flow separation within a scope as close to

* Corresponding author.
E-mail addresses: timothee.chabert@onera.fr (T. Chabert), julien.dandois@onera.fr (J. Dandois), eric.garnier@onera.fr (É. Garnier), laurent.jacquin@onera.fr (L. Jacquin).

http://dx.doi.org/10.1016/j.crme.2014.01.013
1631-0721/

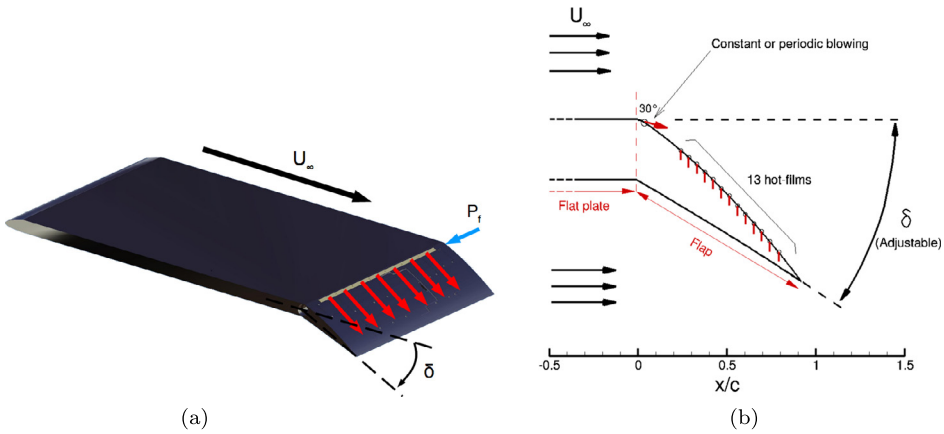

Fig. 1. (Color online.) (a) Wind tunnel model and (b) schematic view of hot films' position.

real application as possible. Therefore, several studies ([3–7]) concerning closed-loop control of flow separation has brought a renewed interest for the research of a detection technique based on wall shear stress. Some authors (Poggie et al. [4] and Shaqarin et al. [6]) propose to base the flow separation detection upon a calibration of the hot films. In this case, the success of flow separation detection relies on the suitable choice of a threshold value that enables one to determine the flow state from the current measurement of wall shear stress. Other authors (Rethmel et al. [5], Packard & Bons [3] and Troshin & Seifert [7]) prefer to use the rms value (or a calculated value assimilated to the rms value) to detect flow separation. Indeed, flow separation is generally marked by a sharp increase of the rms value of hot-film voltage, as shown by Pack et al. [8] and Seifert & Pack-Melton [9]. One advantage of the rms method over the calibration-based method is that the hot films do not need to be calibrated in the former case. Nevertheless, the definition of a threshold on the rms value is still needed in order to determine the flow state according to the rms current value. Furthermore, Nakayama et al. [2] and Meijering & Shroder [10] propose a "two-point" approach since they suggest to calculate the correlation coefficient between the signals of two adjacent hot films. This technique does not need any threshold to be defined since the correlation coefficient is supposed to be simply zero when the flow separation point is located between the two sensors that are considered for detection. However, this method requires two sensors instead of one. Finally, a last detection technique based on the skewness estimation is proposed by Cuvier et al. [11]; this technique is all the more interesting regarding the scope of present study, since it is used to detect flow separation in both uncontrolled and controlled cases.

In the present work, different variables are calculated from the wall shear stress fluctuations measured on the chord of a deflected plain flap on which flow separation naturally occurs. The idea is to evaluate those variables as candidates to define suitable criteria for flow separation detection in both uncontrolled and steady-blowing-controlled cases. The article is divided into three parts. The experimental set-up is first presented in Section 2. In Section 3, the flap is progressively deflected and the natural flow separation that is produced is first revealed through the study of wall pressure distributions. Based on this revelation, wall shear stress fluctuations are studied and the evolutions of several variables calculated from hot-film voltages are linked with the development of flow separation. Then, steady blowing is applied in Section 4 and its impact on wall shear stress fluctuations is studied in order to reveal the flow separation delay due to flow control.

2. Experimental apparatus

The experiments are performed in the S_2L Eiffel-type wind tunnel located at the ONERA Chalais–Meudon research centre. For more details on the experimental set-up, the reader can refer to Ref. [12]. The test model is presented in Fig. 1(a) and consists of an 867-mm-long flat plate and a plain flap (chord length $c = 220$ mm), based on a NACA 4412 airfoil shape. It is placed inside a cylindrical slightly divergent 1750-mm-long test section. The model covers the 800 mm of the wind tunnel span. Carborundum is used at its leading edge to trigger transition. Surface-oil-flow visualisations have shown that the set-up is two dimensional on 80% of the span. The wind tunnel tests are performed at an average free-stream velocity $U_\infty = 24.5\ \mathrm{m\,s^{-1}}$, giving a Reynolds number $Re_{\mathrm{model}} = 2 \cdot 10^6$ based on the total length of the model. The external turbulence level is 0.2% (see Gand et al. [13] and Brion [14]). The wind tunnel model is installed with a zero angle of attack and the flap can be deflected by a positioning system according to the angle δ from 2 to 37°. The deflection angle is denoted by δ. Thirteen Senflex® hot-film sensors are chordwise (single row) and regularly bonded on the flap (see Fig. 1b). They are regulated by three Dantec® *Streamlines* and the corresponding voltage signals are simultaneously acquired and digitised by a NI PXIe-6358 data acquisition card at a sampling rate of 10 kHz. The signals are low-pass filtered at 3 kHz to avoid aliasing. The signal acquisition lasts for 40 s. Welch's periodogram method is used to estimate the power spectral densities presented in the following. The signals are divided into 79 blocks with 50% overlap, so the resolution is of 0.6 Hz.

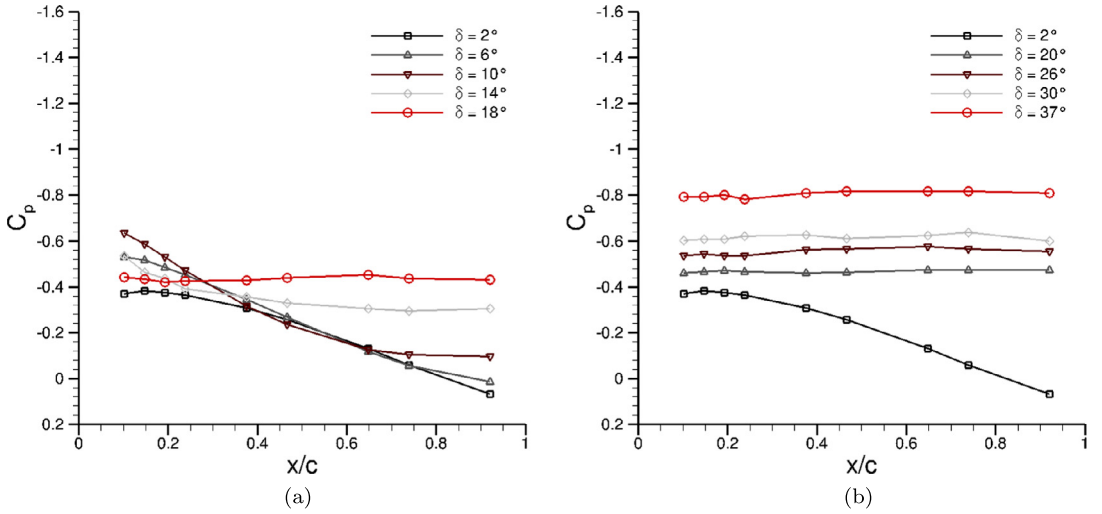

Fig. 2. (Color online.) Pressure coefficient C_p distributions for different flap deflection angles. Results are presented on two plots for the sake of clarity.

Seven blowing slots are integrated into the leading edge of the flap and along its whole span. They are 0.25-mm-wide and 90-mm-long and share a common pipe of compressed air. The pneumatic circuit enables one to get a constant feeding pressure of 7 bar during all the experiments for which steady blowing is applied. The slots are separated from each other by 7 mm (0.9% of the span) and cover 80% of the total span. The jets blow with a fixed angle of 30° with respect to the local flap tangent, as indicated on the schematic view presented in Fig. 1b.

As recalled in the introduction, the ability of constant blowing to reattach a separated boundary layer is classically quantified by the momentum coefficient, denoted by c_μ and defined as (see Ref. [15])

$$c_\mu = \frac{q_\mathrm{m} U_\mathrm{j}}{\frac{1}{2}\rho_\infty U_\infty^2 S_0} = \frac{\rho_\mathrm{j} U_\mathrm{j}^2 S_\mathrm{j}}{\frac{1}{2}\rho_\infty U_\infty^2 S_0}, \tag{1}$$

where U_j is the jet exhaust velocity and q_m the mass flow rate ejected through the actuators. S_j and S_0 are the slots' surface and the reference surface, respectively. ρ_j and ρ_∞ are the densities at the slot exit and of the free stream, respectively. The reference surface is defined as the flap surface. This reference surface definition leads to momentum coefficients greater than the ones generally obtained for similar configurations (e.g., Becker et al. [16]), where the surface of the whole model is taken as a reference.

3. Uncontrolled flow

3.1. Analysis of wall pressure distributions

Fig. 2 presents the distributions of the pressure coefficient C_p for different flap deflection angles ranging from 2 to 37°. No control is applied. Pressure coefficient is defined as

$$C_p = \frac{p - p_\infty}{\frac{1}{2}\rho_\infty U_\infty^2}, \tag{2}$$

where p is the static pressure on the model wall and p_∞ the freestream static pressure.

In Fig. 2a, one can observe that the flow is attached on the flap when deflected at $\delta = 2°$. A plateau of C_p is progressively developing from the trailing edge towards the leading edge as the flap deflection angle increases. This plateau of pressure coefficient reveals the development of a recirculation zone which progressively grows over the flap. When flap deflection reaches $\delta = 18°$, the plateau of C_p clearly extends from $x/c = 0.239$ to the flap trailing edge. The part close to the leading edge, i.e. from $x/c = 0$ to $x/c = 0.239$, still exhibits a slight gradient of C_p. Therefore, it is difficult to conclude whether the flow is still partly attached or fully separated in that case. When the flap is deflected at $\delta = 20°$, the flow is fully separated (see Fig. 2b), since the plateau of C_p covers the entire flap. Fig. 12a presents the visualisation of the flow when the flap is deflected at $\delta = 20°$ and confirms that the flow is fully separated at that deflection angle. The lack of pressure taps close to the flap hinge prevents one from accurately calculating the lift coefficient of the wind-tunnel model. Nevertheless, an estimate of the 2D-profile lift coefficient, denoted by C_L^*, is calculated on the whole model according to

$$C_\mathrm{L}^* = \int_0^1 \left(C_p^- - C_p^+\right) \mathrm{d}\left(\frac{x}{c_t}\right), \tag{3}$$

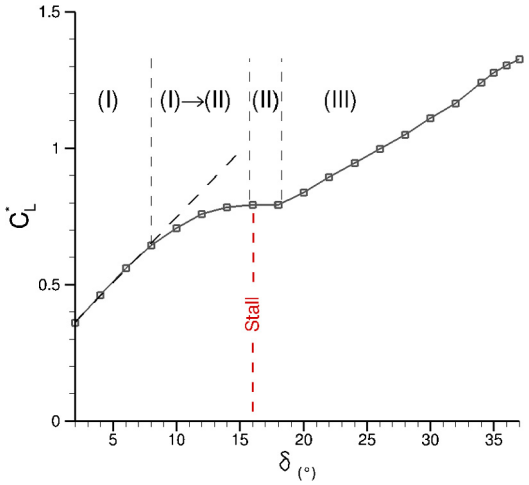

Fig. 3. (Color online.) Evolution of the estimated lift coefficient C_L^* as a function of the flap deflection angle δ for a zero angle of attack ($i = 0°$; $c/c_t = 20\%$; no control).

where C_p^+ and C_p^- are the pressure coefficients on the suction side and the pressure side, respectively; c_t is the chord length of the entire model (flat plate and flap). Fig. 3 presents the estimated lift coefficient C_L^* as a function of the flap deflection angle δ. In our case, the flap chord ratio is $c/c_t = 20\%$.

The curve is identical to the one reported by Hoerner [17] for the same flap chord ratio ($c/c_t = 20\%$) and an equivalent Reynolds number. Three regions can be drawn out of this curve, as proposed by Williamson [18]. The first region, denoted by (I) in Fig. 3, extends from $\delta = 2°$ to $\delta = 10°$ and is characterised by the linear evolution of C_L^* as a function of flap deflection. The transition from region (I) to region (II), which extends from 8 to 16°, is marked by a progressive rounding of the lift curve. In the case reported by Hoerner[17], this transition is marked by a sharp stop of the C_L increase. However, in the present case, this transition is progressive. This means flow separation develops progressively when the flap is deflected. From $\delta = 16°$ to $\delta = 18°$, the lift coefficient does not evolve any more since a recirculation bubble covers the whole flap. By analogy with the classic lift curve, it is possible to define a stall angle which is equal to $\delta_s = 16°$ in our case. It has to be noted that lift increases once again after stall, defining a third region denoted by (III) in Fig. 3. This last region corresponds to a non-linear increase of the lift coefficient C_L^*. In our case, region (III) appears to be almost linear because the flap deflection angle is not high enough in comparison with the case of Williamson [18], where the deflection is increased to 70°, and the cases reported by Hoerner [17], where deflection increases towards 90°.

3.2. Analysis of the wall shear stress spectra on the flap

Fig. 4 presents the weighted power spectral density $f \cdot G(f)$ as a function of the flap deflection angle δ for flap chord positions $x/c = 0.239$, $x/c = 0.420$, $x/c = 0.648$, and $x/c = 0.739$. The spectra are calculated from 40-s-long hot-film signals, while the flap deflection angle remains constant. The spectral density of wall shear stress fluctuations changes when the flap deflection angle is increased, and those changes depend on the flap chord position. The three regions drawn from the lift increment plot presented in Fig. 3 can be found again in the spectral density evolutions. They are described in details hereinafter.

3.2.1. Progressive separation

For $\delta < 14°$, the wall shear stress fluctuations inside the 100–300-Hz frequency range are amplified when the flap deflection angle reaches a given value that depends on the chord position. For each chord position presented in Fig. 4, the horizontal black line marks the flap deflection angle for which the maximum of power spectral density is reached for angles below 14°. This high level of fluctuations reveals the presence of the flow separation point on the corresponding hot film. More specifically, this occurs before the flow separation point crosses the considered hot-film location. The C_p distributions previously presented leads to a first estimate of flow separation mean location for each tested deflection angle. This estimation can be done by approximately determining the position where the C_p gradient becomes zero. For example, it is possible to estimate that the flow separation point is located at $x/c = 0.739$ on average when the flap deflection is $\delta = 6°$. At the same chord position, the power spectral density presented in Fig. 4(d) reveals high levels of fluctuations when $\delta = 5°$. The same statement can be drawn for other flap deflections. The amplification of wall shear stress fluctuations within the 100–300-Hz frequency range appears then as a precursor to flow separation. This result was already reported by Seifert and Pack-Melton [9] and Simpson et al. [19], but for pressure fluctuations in the latter case.

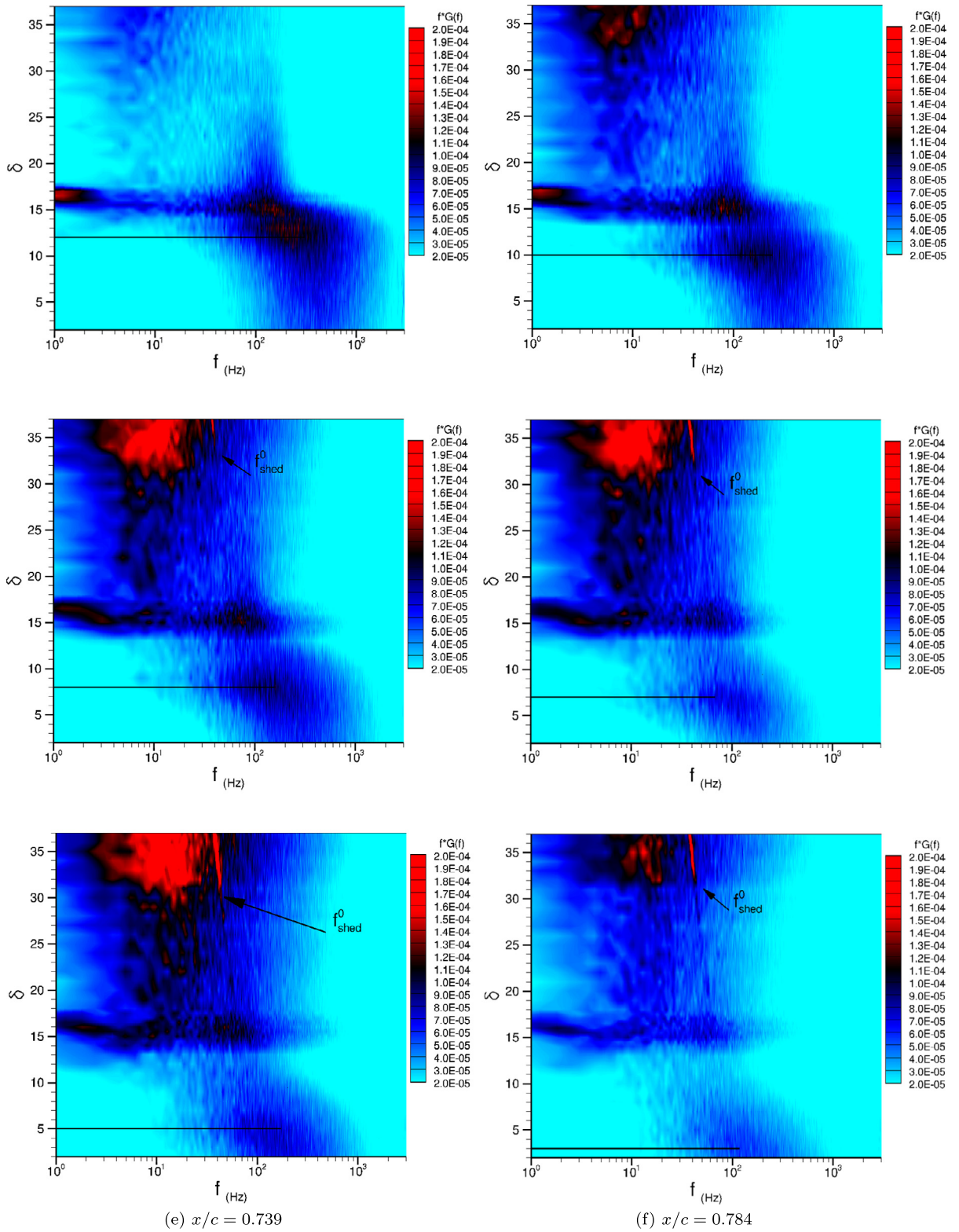

(e) $x/c = 0.739$ (f) $x/c = 0.784$

Fig. 4. (Color online.) Weighted power spectral density $f \cdot G(f)$ of wall shear stress fluctuations as a function of the flap deflection angle δ for chord positions (a) $x/c = 0.239$, (b) $x/c = 0.420$, (c) $x/c = 0.557$, (d) $x/c = 0.648$, (e) $x/c = 0.739$, and (f) $x/c = 0.784$ (no control).

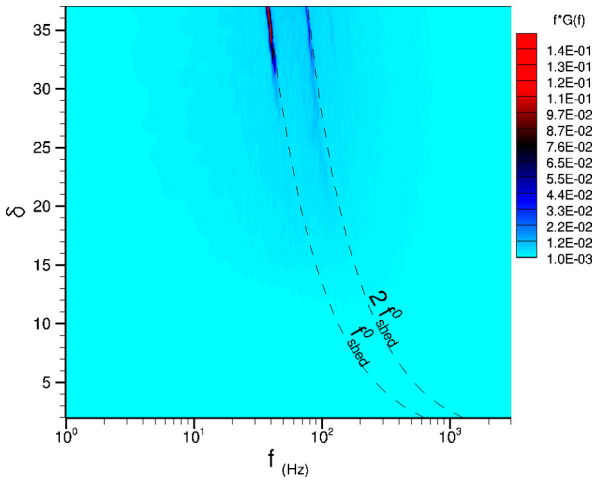

Fig. 5. (Color online.) Weighted power spectral density $f \cdot G(f)$ of streamwise velocity fluctuations measured in the wake as a function of the flap deflection angle δ.

3.2.2. Stall region

For $15 \leq \delta \leq 17°$ and whatever the flap chord x/c position, there is a high level of wall shear stress fluctuations on a large frequency band, i.e. from 1 to around 500 Hz. This happens when the flap deflection is around the stall angle which was determined previously from the results presented in Fig. 3. This region marks a transition from high to low frequencies, the latter ones characterising the separated flow. Moreover, a low-frequency peak located at around 1 Hz appears in the power spectral density for chord positions close to the leading edge, i.e. $x/c = 0.239$ and $x/c = 0.420$. It is not easy to find the origin of this low-frequency phenomenon. Indeed, it appears when the flow separation point reaches the leading edge of the flap. The low-frequency phenomenon already described by Zaman et al. [20] (see also Almutairi and AlQadi [21]) shares common facts with the one observed in the present study. In the case of Zaman et al. [20], it corresponds to an alternative change between attached and separated flow states for a 2D-profile at $Re_c = 10^5$ and approaching stall. This oscillation between the two states does not correspond to the Von Kármán vortex shedding (see the explanation about Fig. 5) and is quickly dampened for increasing flap chord positions.

Further investigations would be necessary to fully explain this phenomenon, but they lie beyond the scope of the present study.

3.2.3. Post-stall flow

Close to the trailing edge, i.e. for $x/c = 0.648$ and $x/c = 0.739$ among the flap chord positions chosen and presented in Fig. 4, a sharp peak located at the vortex shedding frequency appears beyond $\delta = 32°$. The natural vortex shedding frequency is denoted by f^0_{shed} (notation introduced by Wu et al. [22]). The frequency observed in Fig. 4 corresponds to a Strouhal number $St_{\text{shed}} = 0.2$; its value is obtained from the equation

$$St_{\text{shed}} = \frac{f^0_{\text{shed}} c \sin(\delta)}{U_\infty}. \tag{4}$$

Fig. 5 presents the weighted power spectral density $f \cdot G(f)$ of streamwise velocity fluctuations in the wake (i.e. acquired by a hot wire located $3c$ downstream from the wind-tunnel model). Theoretical values of vortex shedding f^0_{shed} and of its first harmonic $2 f^0_{\text{shed}}$ are also plotted for all tested deflection angles. In the wake, Von Kármán vortex shedding appears clearly for flap deflection angle higher than 32°; it was also the case for wall shear stress fluctuations close to the trailing edge (see Fig. 4). The first harmonic $2 f^0_{\text{shed}}$ appears for the same deflection angles as well. In both cases, the values obtained experimentally are very close to the theoretical ones calculated with Eq. (4).

3.2.4. Summary of the three phases and separation criteria

Up to now, the progressive flow separation occurring on the flap has been characterised through pressure distribution measurements and the evolution of the frequency content of velocity and wall shear stress fluctuations. Fig. 6 presents the standard deviation σ value of wall shear stress fluctuations as a function of the flap chord position x/c and of the flap deflection angle δ. It is calculated from 40-s-long hot-film signals acquired during experiments where the flap deflection angle remains constant and sampled at 10 kHz.

The high level of fluctuations inside the 100–300-Hz frequency range observed in Fig. 4 results in a rms value peak that moves from the trailing to the leading edge as the flap deflection increases. The evolution of this peak is indicated by a series of black squares in Fig. 6. These peaks mark the displacement of the flow separation point on the flap chord. A second rms value peak is more pronounced than the first one, and covers the entire flap chord for $15 \leq \delta \leq 17°$. It marks

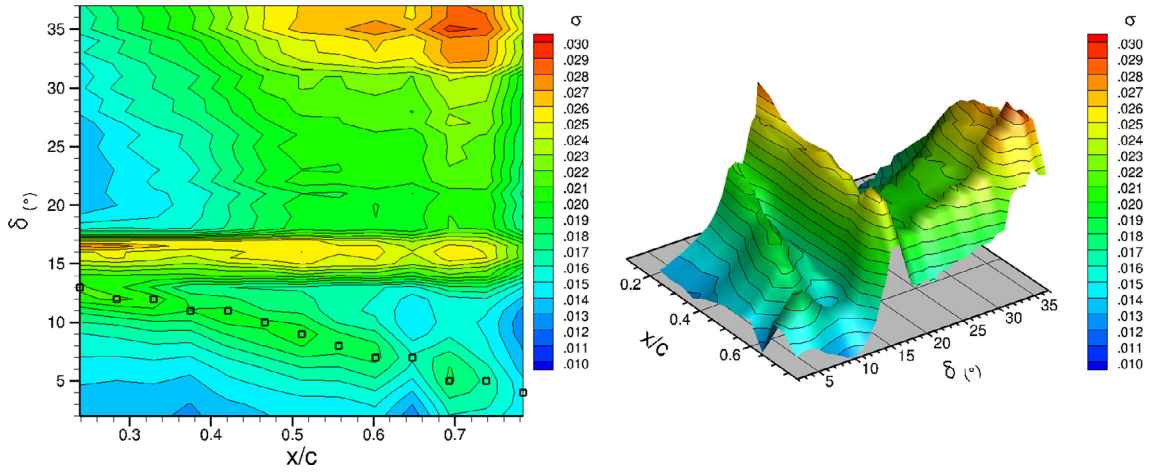

Fig. 6. (Color online.) Standard deviation σ of wall shear stress fluctuations as a function of the flap chord position x/c and the deflection angle δ, in (a) 2-D and (b) 3-D.

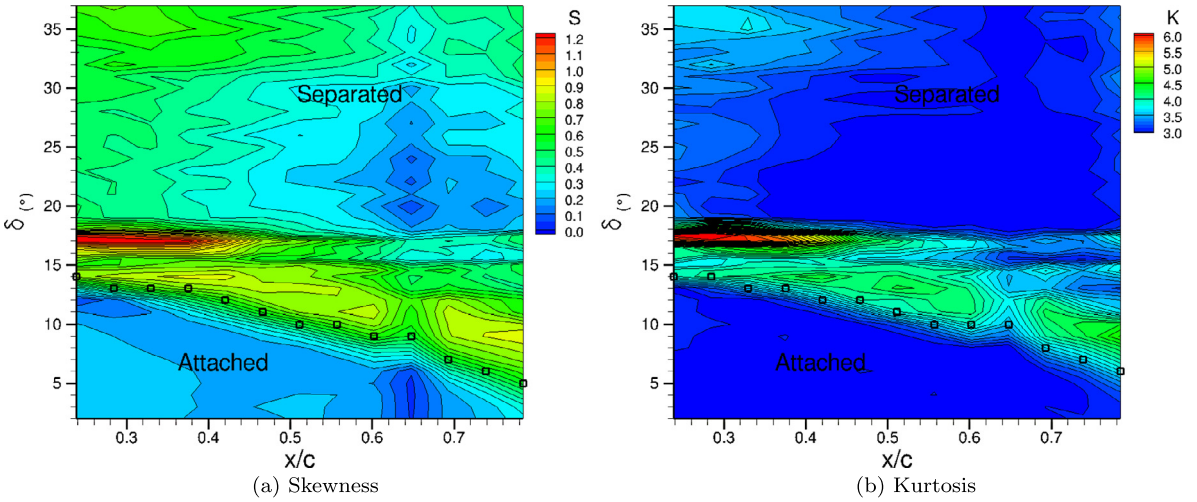

Fig. 7. (Color online.) (a) Skewness S and (b) kurtosis K of wall shear stress fluctuations as functions of the flap chord position x/c and of the deflection angle δ.

the large frequency band's high level of wall shear stress fluctuations already observed in Fig. 4 when the flap approaches stall. This second peak is still present, even if the rms value is calculated on the 100–300-Hz frequency band (not presented here). The rise of rms value occurring for high deflections ($\delta \geq 32°$) and close to the trailing edge $x/c \geq 0.6$ corresponds to the development of vortex shedding. Fig. 7 presents the maps of statistical moments of order 3 and 4, i.e. skewness and kurtosis, respectively. Those moments are plotted as a function of the flap chord position x/c and of the flap deflection angle δ. Each moment is calculated on 40-s-long hot-film signals sampled at a rate of 10 kHz.

The progressive flow separation is marked by a sharp rise of both skewness S and kurtosis K. Especially, the third statistical moment rises from values around 0.2 to values higher than 0.5 when the deflection angle δ increases and for a given chord position x/c. It decreases then towards values around 0.3–0.4. On the contrary, kurtosis falls back to its initial values around 3. To follow flow separation extension when the flap deflection angle increases, thresholds at 0.5 and 3.5 are chosen for skewness and kurtosis, respectively. A more comprehensive discussion about flow separation detection by skewness and kurtosis monitoring is made in Ref. [12].

3.3. Analysis of coherence

3.3.1. Evolution of the location of the separation point

Fig. 8 presents the evolution of the coherence function γ^2 against the flap deflection angle δ.

The coherence function map is presented for four couples of hot films, $x/c = [0.239–0.284]$, $x/c = [0.375–0.420]$, $x/c = [0.602–0.648]$ and $x/c = [0.739–0.784]$. For each hot-film couple, the coherence first reaches high values close to 0.7

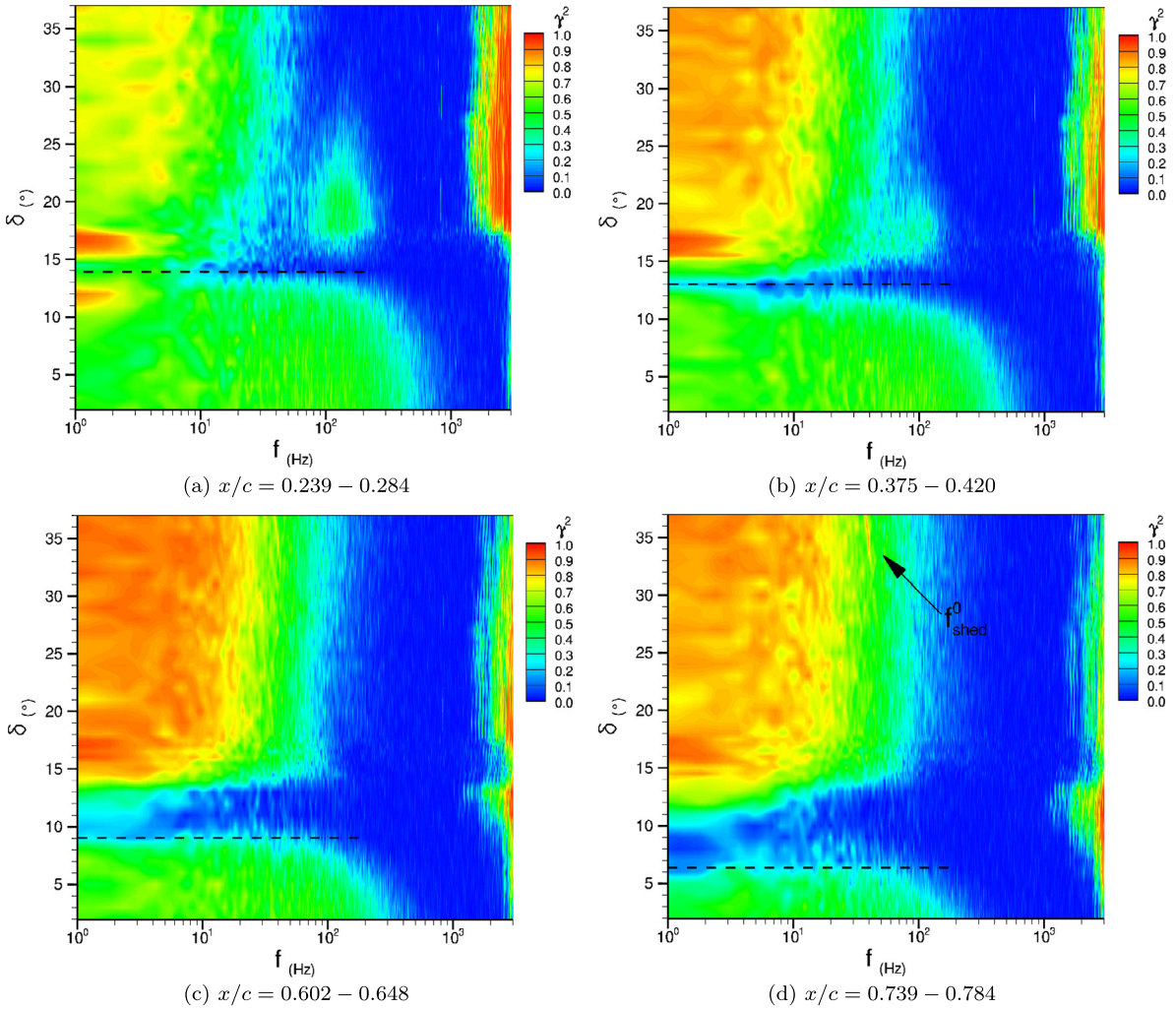

(a) $x/c = 0.239 - 0.284$ (b) $x/c = 0.375 - 0.420$

(c) $x/c = 0.602 - 0.648$ (d) $x/c = 0.739 - 0.784$

Fig. 8. (Color online.) Coherence function γ^2 against flap deflection angle calculated between the four couples of hot-film signals: $x/c = [0.239–0.284]$, $x/c = [0.375–0.420]$, $x/c = [0.602–0.648]$, and $x/c = [0.739–0.784]$.

for low angles of deflection on the frequency band extending from 1 to almost 500 Hz (attached boundary layer). Then, the coherence falls to values close to 0. This coherence fall happens when the deflection angle reaches a given value depending on the flap chord position and reveals a change in close-wall flow direction. Thus, the loss of coherence marks the current location of the flow separation point. Moreover, the range of flap deflection angles where the coherence is almost 0 is larger for chord positions close to the trailing edge. This suggests the location of the flow separation point fluctuates when this point is still close to the trailing edge, and it fluctuates less and less as the flap deflection angle increases and the flow separation gets closer to the leading edge. Once the flow separation point has passed, coherence largely increases towards values higher than 0.9. Besides, coherence is high but on a limited frequency band in comparison with the attached case, because the separated zone is characterised by frequencies lower than the ones that are observed in the attached zone (see Fig. 4). By the way, the development of vortex shedding in the wake is also marked in the evolution of the coherence function between the two hot films located at $x/c = 0.739$ and $x/c = 0.784$ for flap deflection angles higher than 20°. Finally, one can observe a sharp increase of coherence for frequencies higher than 2000 Hz. This increase does not originate from flow physics and is most certainly due to the hot-film temperature control which induces sometimes high-frequency resonance.

3.3.2. Separation criteria

In order to follow the evolution of flow separation when the flap deflection angle increases, the coherence function is summed (integrated) on the 1–200-Hz frequency band for each tested deflection angle and each chord position according to the equation

$$s = \int_{1}^{200} \gamma^2(f)\,\mathrm{d}f. \tag{5}$$

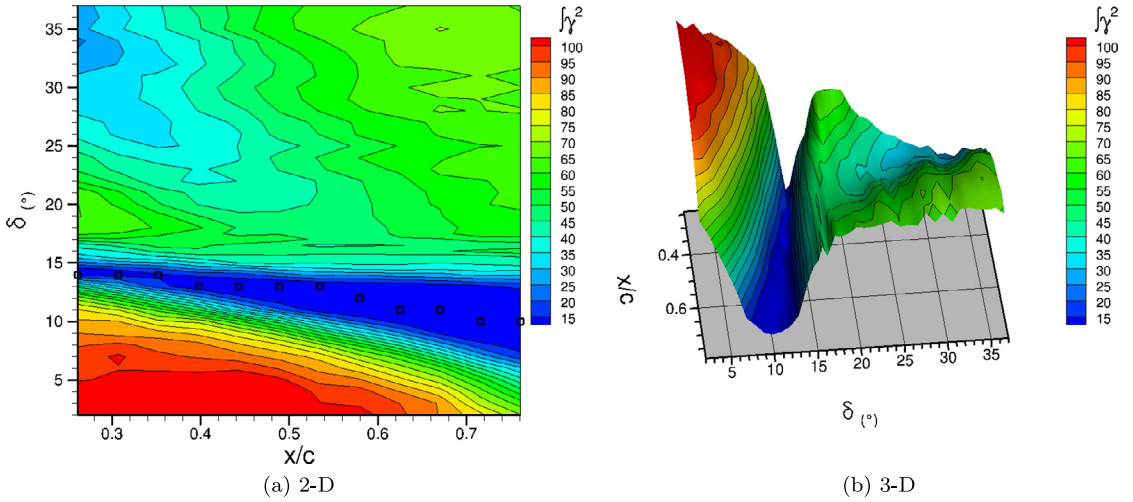

Fig. 9. (Color online.) Sum of coherence function $\int \gamma^2$ on the 1–200-Hz frequency band (see Eq. (5)) as a function of the chord position x/c and the flap deflection δ, in (a) 2-D and (b) 3-D.

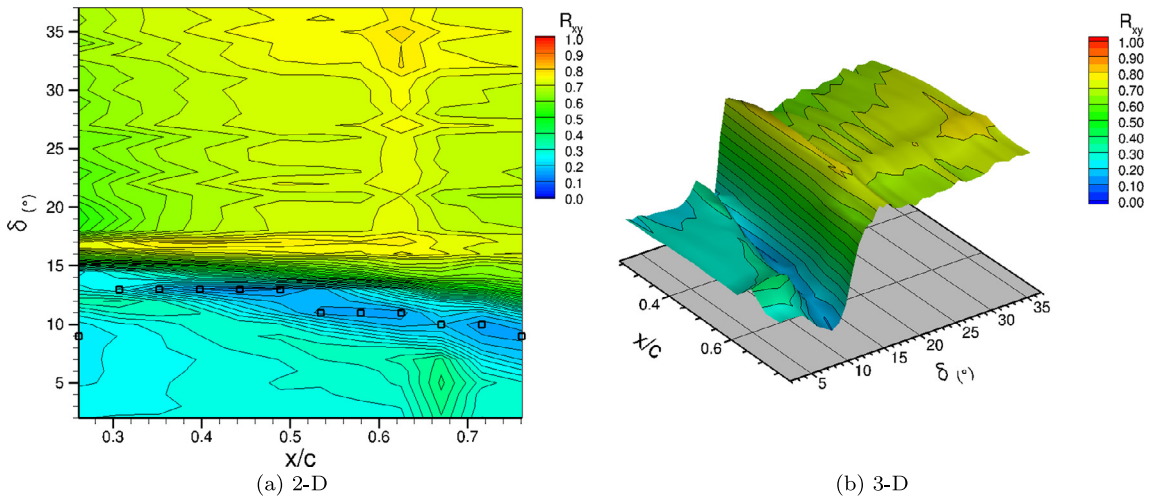

Fig. 10. (Color online.) Correlation coefficient R_{xy} as function of chord position x/c and flap deflection δ, in (a) 2-D and (b) 3-D.

The result is plotted as a function of the chord position x/c and the flap deflection δ in Fig. 9. It has to be noted that, for each deflection angle, there are 12 calculated points for variable s. Each one of those points is located between the positions of the two corresponding hot films. The integrated value of coherence s reveals once again the progressive displacement of the flow separation point before stall, which is marked here by a sharp rise of s around $\delta = 16°$. The region where the integrated value of coherence s is minimum is of triangular shape, which means that, as seen in Fig. 8, the range of deflection angles for which coherence is minimum is more and more reduced as flow separation gets closer to the leading edge.

Fig. 10 presents the correlation coefficient denoted by R_{xy} calculated between each couple of adjacent hot films. The correlation coefficient is, in a way, the "temporal equivalent" to coherence. There are 12 correlation coefficients R_{xy} calculated (recall that there are 13 hot-film sensors chordwise distributed on the flap) for each tested deflection angle δ. Correlation coefficients are calculated from 40-s-long hot-film signals and the flap deflection remains constant during the acquisition.

From values around 0.3 at low flap deflection angles, the correlation coefficient first decreases and reaches its minimum, which is close to 0, and then largely increases towards values around 0.7 when the flap deflection angle increases as well. This minimum marks the limit before the inversion in close-wall flow direction (for 2-D flow separation), so it estimates the mean current location of the flow separation point. In other words, there is no more propagation of information between the two hot films that are temporarily situated on both sides of the flow separation point. The two signals that correspond to those hot films are then de-correlated. Therefore, like the coherence (which is the equivalent of correlation in the frequency domain), the progressive displacement of the flow separation point is marked by the correlation coefficient minimum.

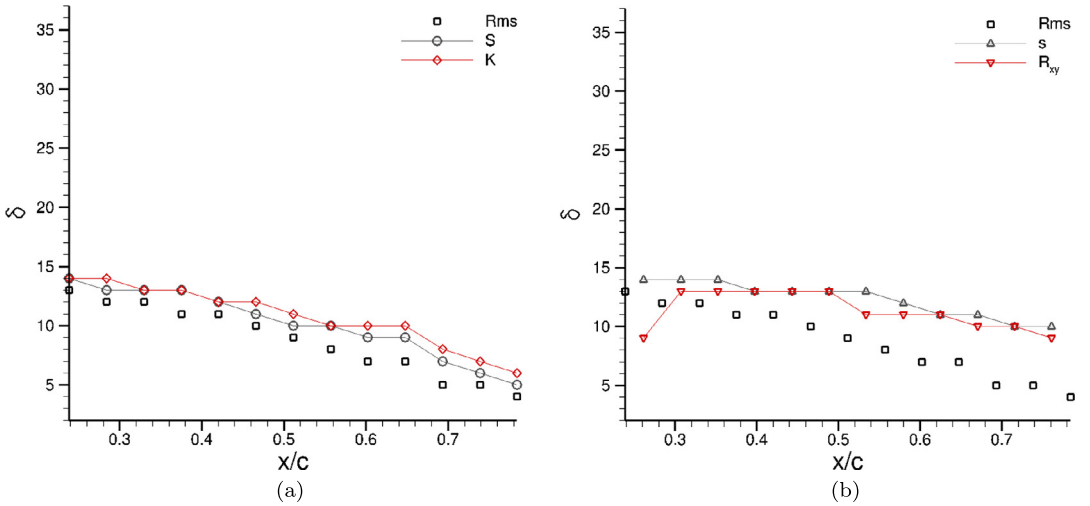

Fig. 11. (Color online.) Summary of the estimated locations of the flow separation point as function of the flap deflection angle δ; those locations are determined from the maps of rms value σ, skewness S, kurtosis K, correlation coefficient R_{xy} and the integrated value s of the coherence function on between 1 and 200 Hz.

3.4. Comparison of the separation criteria

The progressive displacement of the flow separation point has been revealed through different kinds of analysis of pressure, wall shear stress, and velocity measurements. Beyond that, the accurate location of the separation point for a given flap deflection is difficult, since it presupposes the definition of criteria applied to the different statistical and frequency values presented and plotted before. Fig. 11 summarises on two graphs the estimated location of the flow separation point as a function of the flap deflection angle δ; the estimated locations are determined from the maps of rms value σ, skewness S, kurtosis K, correlation coefficient R_{xy} and the integrated value s of the coherence function between 1 and 200 Hz, all presented previously. All those values are able to follow the progressive separation of the flow. Those values are calculated after the event, i.e. they are computed on 40-s-long signals for which the flap deflection angle remains constant. The statistical values calculated on the signal originating from a single hot film (rms, skewness, and kurtosis) are preceding the flow separation in comparison with the values calculated on the signals originating from two adjacent hot films (correlation coefficient and coherence). Nevertheless, all criteria are in good agreement with each other.

As seen in Fig. 3, the progressive flow separation happens between $\delta = 10°$ and $\delta = 16°$. Compared with the results presented in Fig. 11, it appears that the minima of the correlation coefficient and of the coherence function mark the current location of the flow separation point. Thus, the maxima of rms value, skewness and kurtosis are precursors of the separation. Once again, the localisation of the flow separation point as a function of the flap deflection angle is made here *a posteriori* by opposition to a real-time detection.

4. Controlled flow

4.1. Visualisations of the uncontrolled and controlled flows at $\delta = 20°$

Fig. 12 presents the beam-laser tomoscopy visualisations of both uncontrolled and controlled flows when the flap is deflected at 20°. In the controlled case, steady blowing is applied at $c_\mu = 3\%$ ($P_f = 7$ bar). Upstream velocity is still $U_\infty = 24.5\ \mathrm{m\,s^{-1}}$. According to the results of Section 3, the uncontrolled flow is fully separated in the above-mentioned flow conditions.

4.2. Wall shear stress spectra

From a fully separated flow, steady blowing at $c_\mu = 3\%$ is able to entirely suppress the recirculation zone so that the flow is reattached on the whole flap. Fig. 13 presents the weighted power spectral density $f \cdot G(f)$ of wall shear stress fluctuations as a function of the deflection angle δ at flap chord positions (a) $x/c = 0.239$, (b) $x/c = 0.420$, (c) $x/c = 0.648$, and (d) $x/c = 0.739$ when steady blowing is applied at $c_\mu = 3\%$. This figure has to be compared with Fig. 4 presented in the uncontrolled case. Both figures have the same colour scale. (For interpretation of the colour scales in these figures, the reader is referred to the web version of this article.)

The low-frequency content has been entirely removed from the spectrum measured at position $x/c = 0.239$. On the other hand, the rms level of high-frequency fluctuations is much higher than in the uncontrolled case because of the turbulence induced by the steady blowing jet. Thus, steady blowing is able to maintain the flow attached up to position $x/c = 0.239$ and

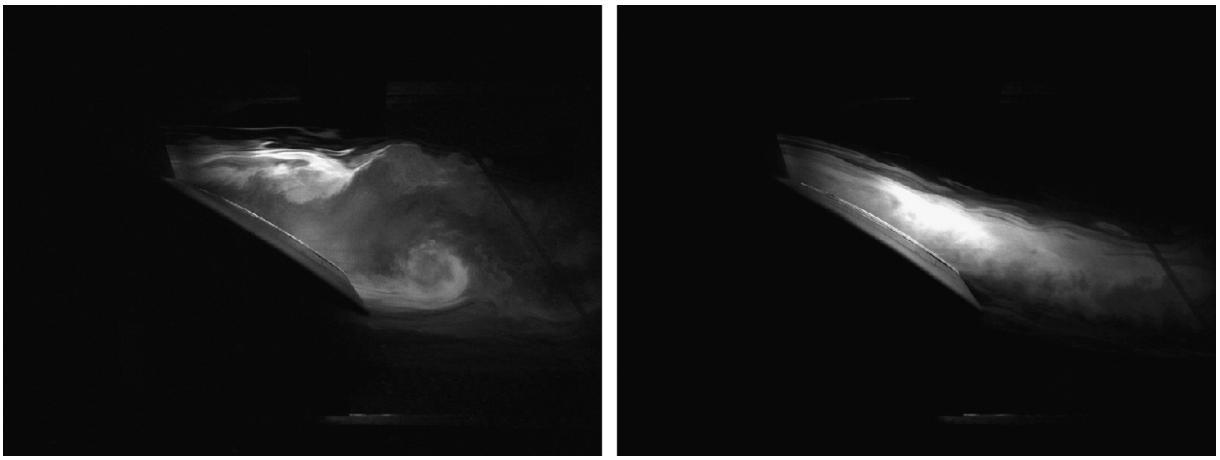

(a) $c_\mu = 0\%$ (b) $c_\mu = 3\%$

Fig. 12. Beam-laser tomoscopy visualisations of the (a) uncontrolled flow and of the (b) flow controlled by steady blowing when the flap is deflected at 20° ($c_\mu = 3\%$).

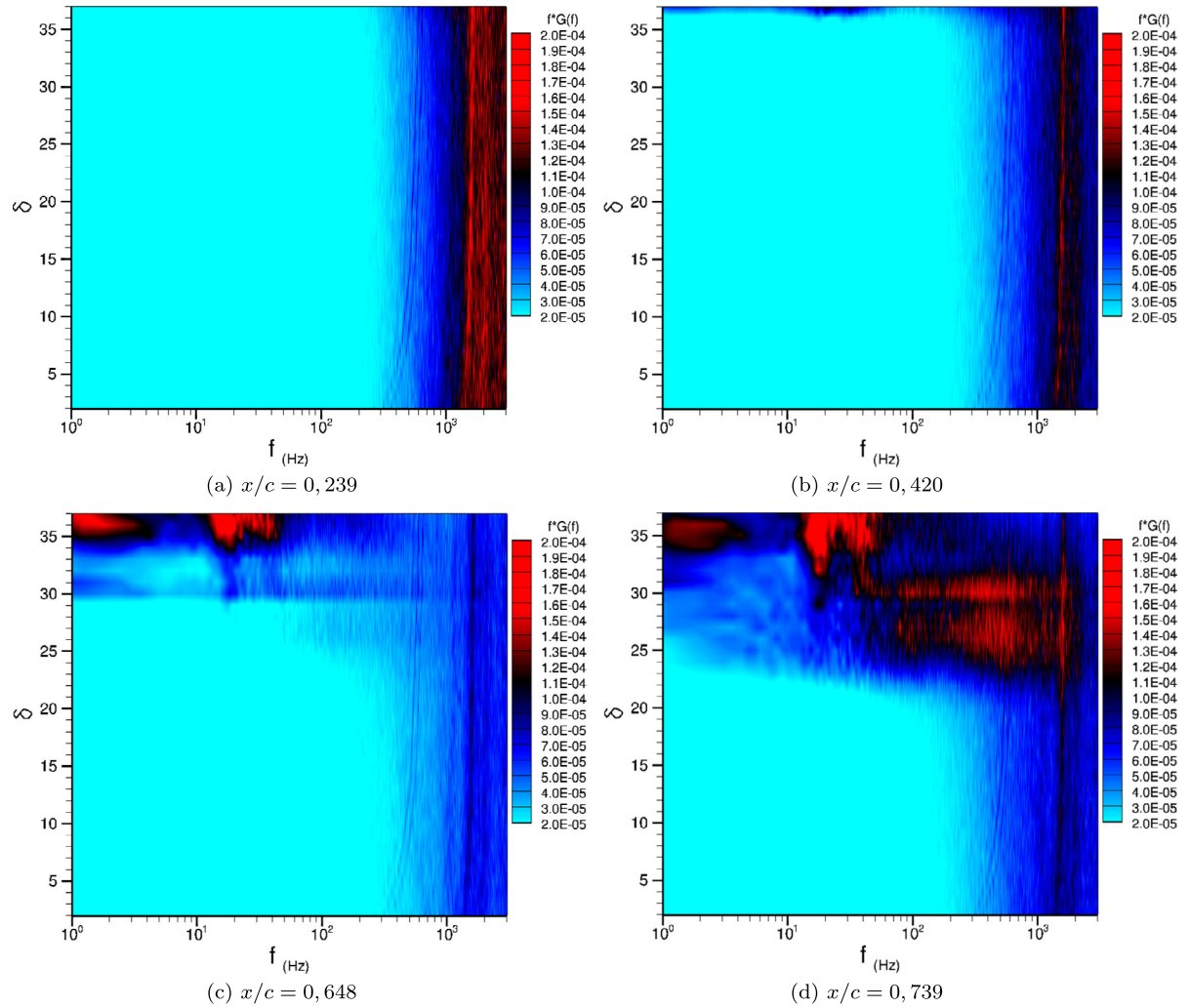

(a) $x/c = 0,239$ (b) $x/c = 0,420$

(c) $x/c = 0,648$ (d) $x/c = 0,739$

Fig. 13. (Color online.) Weighted power spectral density $f \cdot G(f)$ of wall shear stress fluctuations as a function of the deflection angle δ at flap chord positions (a) $x/c = 0.239$, (b) $x/c = 0.420$, (c) $x/c = 0.648$, and (d) $x/c = 0.739$ when steady blowing is applied at $c_\mu = 3\%$.

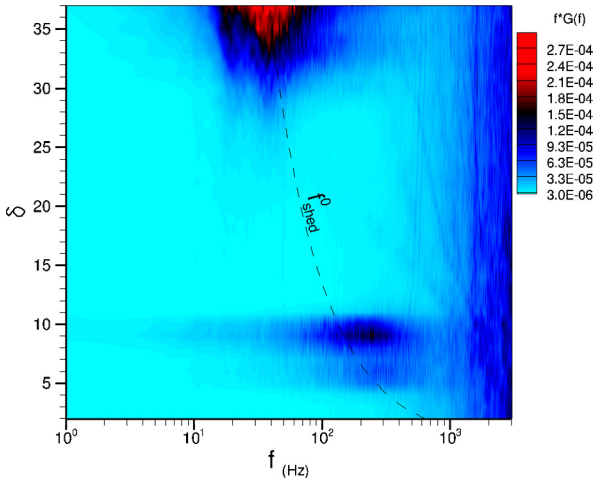

Fig. 14. (Color online.) Weighted power spectral density $f \cdot G(f)$ of velocity fluctuations in the wake as a function of the deflection angle δ when steady blowing is applied at $c_\mu = 3\%$.

flap deflection $\delta = 37°$. On the contrary, a large frequency band content appears in the spectrum measured at $x/c = 0.420$ for flap deflection angles higher than $\delta = 36°$. Closer to the trailing edge, this frequency content appears for lower deflection angles, i.e. for $\delta = 30°$ at position $x/c = 0.648$ and for $\delta = 23°$ at position $x/c = 0.739$. A frequency bump distributed around 30 Hz is developed for deflection angles higher than $\delta = 32°$ and for the two positions that are the closest to the trailing edge. The power spectral density of velocity fluctuations in the wake reveals the same frequency bump around 30 Hz (see Fig. 14). As for shear stress fluctuations, this frequency bump appears for deflection angles higher than $\delta = 32°$. It is actually centred around the theoretical frequency of Von Kármán vortex shedding, even if this one is no more marked by a sharp peak as in the uncontrolled case and for the same deflection angles (see Fig. 5). Finally, as in the uncontrolled case, a low-frequency oscillation (from 1 to 2 Hz) appears for the same flap deflection angle, i.e. for $\delta = 36°$, whatever the position x/c in the separated zone is. Once again, further investigations should be necessary to determine the origin of such low-frequency oscillation.

4.3. Separation criteria

In order to reveal the occurrence of flow separation over the flap when steady blowing is applied, the evolution of standard deviation (integrated value of shear stress fluctuations on the whole spectrum, same as rms value) as a function of flap chord position x/c and deflection angle δ is plotted in Fig. 15. As it could have been expected, the map of rms value reveals the development of the low-frequency shear stress fluctuations at positions close to the trailing edge (those fluctuations are observed in Fig. 13c and d) for flap deflection angles higher than 20°. Flow separation remains localised at positions $x/c > 0.65$ for deflection angles between $\delta = 20°$ and $\delta = 32°$. Then, flow separation extends progressively towards the leading edge when the flap deflection angle increases. By comparing those results with the ones presented in Fig. 6 which presented the rms value map but in the uncontrolled case, it appears that flow separation is effectively delayed thanks to steady blowing.

Fig. 16 presents the evolution of skewness and kurtosis as function of chord position x/c and deflection angle δ when constant blowing is applied. Skewness and kurtosis are still calculated on 40-s-long signals. When control is applied, it appears that flow separation is marked by a decrease of skewness, which falls towards negative values. On the other hand, flow separation is still marked by an increase of kurtosis, but this increase is less sharp than the one observed in the uncontrolled case, for chord positions close to the trailing edge at least. As a consequence, skewness and kurtosis can be considered to be suitable criteria to detect flow separation when steady blowing is applied, but skewness seems more easy to analyse than kurtosis.

In the steady blowing case, flow separation detection by the correlation coefficient or the coherence function failed to clearly detect flow separation; so no results concerning those two criteria are presented here.

5. Conclusion

Flow separation over a plain flap has been studied in this article. Through wall pressure measurements, it has first been shown that flow separation starts from the flap trailing edge and progressively develops towards the leading edge when flap deflection is increased. The study of wall shear stress fluctuations measured by chordwise distributed hot films has led to the definition of several criteria that reveal the extension of flow separation along the chord. The criteria based on the statistical moments that are estimated from a single hot-film signal (rms value, skewness and kurtosis) are precursors

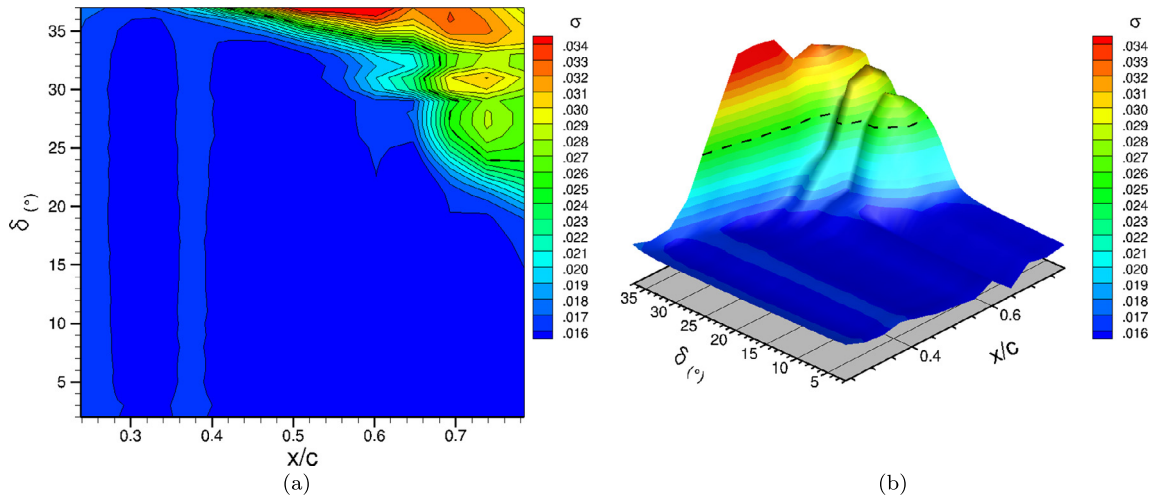

Fig. 15. (Color online.) Rms value of wall shear stress fluctuations as function of chord position x/c and deflection angle δ when steady blowing is applied at $c_\mu = 3\%$.

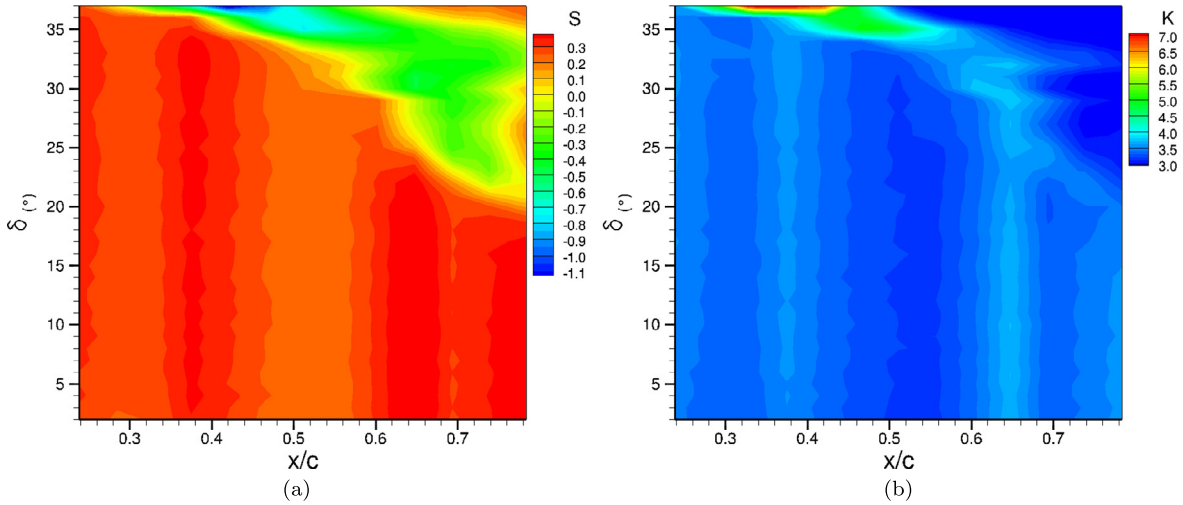

Fig. 16. (Color online.) (a) Skewness and (b) kurtosis of wall shear stress fluctuations as a function of the chord position x/c and of the deflection angle δ when steady blowing is applied at $c_\mu = 3\%$.

of flow separation. On the contrary, the criteria based on the statistics calculated from two hot-film signals (correlation coefficient and coherence) mark the current mean location of the flow separation point.

Concerning the controlled flow, the flow forcing by means of steady blowing at $c_\mu = 3\%$ delays flow separation. All the criteria used in the uncontrolled case have also been tested, but only rms value, skewness and kurtosis have revealed flow separation when steady blowing was applied.

This work provides several criteria to determine *a posteriori* the mean separation location of a turbulent boundary layer by means of wall shear stress measurements. Those criteria are based on the calculation of statistical moments that need a large amount of acquired data to be accurately estimated. The reduction of this amount of data has to be addressed if one of those criteria is to be used as a real-time detector of flow separation within the scope of closed-loop control (see Ref. [23]).

Acknowledgements

The authors would like to acknowledge Michel Alaphilippe and Nicolas Severac for their constant and precious support, and all members of the DAFE PIV team for their help during the tomoscopy experiment.

References

[1] J.P. Stack, S.M. Mangalam, V. Kalburgi, The phase reversal phenomenon at flow separation and reattachment, AIAA Paper 88-0408.

[2] A. Nakayama, J.P. Stack, J.C. Lin, W.O. Valarezo, Surface hot-film method for the measurement of transition, separation, and reattachment points, AIAA Paper 1993-2918.
[3] N.O. Packard, J.P. Bons, Closed-loop separation control of unsteady flow on an airfoil at low reynolds number, AIAA Paper 2012-0754, 2012.
[4] J. Poggie, C.P. Tilmann, P.M. Flick, J.S. Silkey, B.A. Osbourne, Gregory Ervin, D. Maric, S. Mangalam, A. Mangalam, Closed-loop stall control system, J. Aircraft 47 (5) (2010) 1747–1755.
[5] C. Rethmel, J. Little, K. Takashima, A. Sinha, I. Adamovich, M. Samimy, Flow separation control over an airfoil with pulse driven DBD plasma actuators, AIAA Paper 2011-487.
[6] T. Shaqarin, C. Braud, S. Coudert, M. Stanislas, Open and closed-loop experiments to identify the separated flow dynamics of a thick turbulent boundary layer, Exp. Fluids 54 (2013) 1448.
[7] V. Troshin, A. Seifert, Performance recovery of a thick turbulent airfoil using a distributed closed-loop flow control system, Exp. Fluids 54 (2013) 1443.
[8] L.G. Pack, N.W. Schaeffler, C.S. Yao, A. Seifert, Active control of flow separation from supercritical airfoil leading-edge flap shoulder, J. Aircr. 42 (5) (2005) 1142–1149, first presented as AIAA Paper 2002-3156.
[9] A. Seifert, L.G. Pack-Melton, Control and identification of turbulent boundary layer separation, in: Proceedings of the IUTAM Symposium on One Hundred Years of Boundary Layer Research, 2006.
[10] A. Meijering, W. Schroder, Experimental analysis of separated transitional transonic airfoil flow, AIAA Paper 2001-2987.
[11] C. Cuvier, C. Braud, J.-M. Foucaut, M. Stanislas, Flow control over a ramp using active vortex generators, in: Proc. 7th Int. Symp. on Turbulence and Shear Flow Phenomena, 2011.
[12] T. Chabert, J. Dandois, E. Garnier, L. Jacquin, Experimental detection of a periodically forced turbulent boundary layer separation, Exp. Fluids 54 (2013) 1430.
[13] F. Gand, S. Deck, V. Brunet, P. Sagaut, Flow dynamics past a simplified wing body junction, Phys. Fluids 22 (2010) 115111.
[14] V. Brion, Stabilité des paires de tourbillons contra-rotatifs : application au tourbillon de jeu dans les turbomachines, PhD thesis, École polytechnique, Palaiseau, France, 2009.
[15] P. Poisson-Quinton, L. Lepage, Survey of French research on the control of boundary layer and circulation, in: G.V. Lachmann (Ed.), Boundary Layer and Flow Control, vol. 1, Pergamon Press, 1961.
[16] R. Becker, R. King, R. Petz, W. Nitsche, Adaptive closed-loop separation control on a high-lift configuration using extremum seeking, AIAA J. 45 (6) (2007) 1382–1392.
[17] S.F. Hoerner, H. Borst, Fluid-Dynamic Lift, Mrs Liselotte A. Hoerner, Brick Town, NJ, 1975.
[18] G.A. Williamson, Experimental wind tunnel study of airfoils with large flap deflections at low Reynolds numbers, Master thesis, University of Illinois at Urbana-Champaign, IL, USA, 2012.
[19] R.L. Simpson, M. Ghodbane, B.E. McGrath, Surface pressure fluctuations in a separating turbulent boundary layer, J. Fluid Mech. 177 (1987) 167–186.
[20] K.B.M.Q. Zaman, D.J. McKinzie, C.L. Rumsey, A natural low-frequency oscillation of the flow over an airfoil near stalling conditions, J. Fluid Mech. 202 (1989) 403–442.
[21] J.H. Almutairi, I.M. AlQadi, Large-eddy simulation of natural low-frequency oscillations of separating – reattaching flow near stall conditions, AIAA J. 51 (4) (2013) 981–991.
[22] J.-Z. Wu, X.-Y. Lu, A.G. Denny, M. Fan, J.-M. Wu, Post-stall flow control on an airfoil by local unsteady forcing, J. Fluid Mech. 371 (1998) 21–58.
[23] T. Chabert, Contrôle expérimental en boucle fermée du décollement sur un volet, PhD thesis, Université Pierre et Marie Curie, Paris VI, France, 2014.